ADVANCED ELECTRONIC MATERIALS Open Access
www.advelectronicmat.de

Check for updates

Glassy Synaptic Time Dynamics in Molecular $La_{0.7}Sr_{0.3}MnO_3$/Gaq_3/AlO_x/Co Spintronic Crossbar Devices

*Andrei Shumilin, Prakriti Neha, Mattia Benini, Rajib Rakshit, Manju Singh, Patrizio Graziosi, Raimondo Cecchini, Luca Gnoli, Mirko Prezioso, Ilaria Bergenti, Valentin Alek Dediu, and Alberto Riminucci**

The development of neuromorphic devices is a pivotal step in the pursuit of low-power artificial intelligence. A synaptic analog is one of the building blocks of this vision. The synaptic behavior of molecular $La_{0.7}Sr_{0.3}MnO_3$/tris(8-hydroxyquinolinato)gallium/AlOx/Co spintronic devices is studied, where the conductance plays the role of the synaptic weight. These devices are arranged in a crossbar configuration, the most effective architecture for the purpose. The conductance of each cross point is controlled separately by the application of voltage pulses: when set in the high conductance potentiated state, the devices show a spin-valve magnetoresistance, while in the low conductance depressed state, no magnetoresistance is observed. The time dependence of the resistive switching behavior is an important parameter of the synaptic behavior and is very revealing of the underlying physical mechanisms. To study the time dynamics of the resistive switching after the voltage pulses, the response of the device to trains of potentiation and depression pulses, and the time-resolved conductivity relaxation after the pulses are measured. The results are described with the conductivity model based on impurity energy levels in the organic semiconductor's gap. A flat distribution of the activation energies necessary to move these impurities is hypothesized, which can explain the observed glassy behavior.

1. Introduction

Artificial intelligence (AI) has fast become one of the most important developments in the ongoing information-age revolution. Approaches vary from classical symbolic AI[1] to the more biologically inspired algorithms used in neural networks.[2]

Since its inception, AI has taken inspiration from naturally intelligent entities like brains, neurons, and synapses. Brain-inspired AI, also known as neuromorphic computing, tries to study the brain's structure to work out what are the mechanisms that confer its intelligence.[3]

One of the basic functional anatomical features of the brain is the synapse, a small area of a neuron's receiving dendrites that connects it to another neuron's outgoing axon; the synapse is believed to be one of the building blocks of the brain's intelligence.[4] Its behavior was mimicked by the earliest computer algorithms aiming at implementing some form of intelligence, such as the perceptron and backpropagation.[5] One of the defining features of the synapse is its plasticity, which is believed to confer the brain its ability to learn. It is obtained by 2 opposing phenomena, potentiation, consisting in a strengthening of the connection between 2 neurons, and depression, consisting in its weakening.

Simulating synapses to perform neuromorphic computing on a conventional computer program means having to deal with

A. Shumilin
Jozef Stefan Institute
Jamova 39, Ljubljana SI-1000, Slovenia

R. Cecchini
Institute for Microelectronics and Microsystems (IMM)
CNR
Via Gobetti 101, Bologna 40129, Italy

The ORCID identification number(s) for the author(s) of this article can be found under https://doi.org/10.1002/aelm.202300887

© 2024 The Authors. Advanced Electronic Materials published by Wiley-VCH GmbH. This is an open access article under the terms of the Creative Commons Attribution License, which permits use, distribution and reproduction in any medium, provided the original work is properly cited.

DOI: 10.1002/aelm.202300887

P. Neha
Microelectronics Research Center
University of Texas
Austin, TX 78758, USA

P. Neha, M. Benini, R. Rakshit, M. Singh, P. Graziosi, L. Gnoli, M. Prezioso, I. Bergenti, V. A. Dediu, A. Riminucci
Institute for the Study of Nanostructured Materials (ISMN)
CNR
Via Gobetti 101, Bologna 40129, Italy
E-mail: alberto.riminucci@cnr.it

M. Prezioso
Mentium Technologies Inc. 3448 Elings Hall
University of California
Santa Barbara, CA 93106, USA

the memory access bottleneck[6] that slows down performance and increases the energy budget. In order to achieve performances comparable to the brain's, especially in terms of energy efficiency, it is necessary to resort to hardware neuromorphic implementations.[7] The foremost approach in solid-state physics consists in using resistive switching devices,[8] in which the strength of the synapse is embodied in their conductance. Resistive switching devices can retain their state without any power having to be supplied, in contrast with conventional SRAMs and DRAMs. Their conductance, and therefore the strength of the synapse, is usually changed by the application of a voltage pulse. Several technologies can achieve this behavior.[9]

Different materials were proposed to fabricate artificial synapses. Each has unique potentiation/depression dynamics that follow from the physical phenomena underlying the switching process. These properties provide both limitations and opportunities for device fabrication.[9] In phase change memory-based devices, the potentiation dynamics are controlled by melting and recrystallization of the contact part of the device, leading to a switching delay time that is dependent on the pulse amplitude.[10] In ferroelectric devices, the process is controlled by domain dynamics.[11] In valence change memories the potentiation is often described in terms of filament formation.[12] This leads to the preliminary filament-forming pulse required for device operation and to the gradual response to a train of weak pulses.[13] The filament can dissolve over time, which allows to use of the device as a short-term dynamical element in a neuromorphic circuit. In polymer electrochemical neuromorphic devices, the trains of pulses are accompanied by the paired-pulse facilitation slowly decaying in time.[14]

Here we use the unique combination of the molecular semiconductor tris(8-hydroxyquinolinato)gallium (Gaq3) and a valence change memory material (AlOx) comprised between 2 ferromagnetic electrodes, thus forming a molecular spin valve. In this way, we add a second means to control the conductance of the synaptic devices, that is the magnetic field. The molecular spin valve shows both conventional resistive switching and magnetoresistance: by sweeping an applied magnetic field, the magnetizations of its ferromagnetic electrodes can be set either parallel, corresponding to a low conductance state, or antiparallel, corresponding to a high conductance state.[15,16] The addition of this degree of freedom speeds up the learning rate in a simulation based on a reinforcement learning algorithm.[17]

In this article, we study the time dynamics of the resistive switching properties of $La_{0.7}Sr_{0.3}MnO_3$(LSMO)/ Gaq3/AlOx/Co molecular spin valves, arranged in a 4 × 3 crossbar configuration. We demonstrate that the resistive state of each cross-point can be changed progressively in a non-volatile fashion by the application of a voltage pulse. We demonstrate that the crosstalk between the addressed junction and the other ones was 8% on average. We show that the dynamics are logarithmic overtime over 3 different time scales: after the application of voltage pulse, over the repetition of identical voltage pulses, and over the repetition of the latter experiments. Such dynamics are known from the literature to increase the efficiency of learning algorithms for spiking neural networks (SNN).[18] Finally, we provide a physical model of the synaptic behavior of our devices, adding insight into the microscopic origin of the resistive switching, that is attributed to the migration of oxygen-doping species.[19]

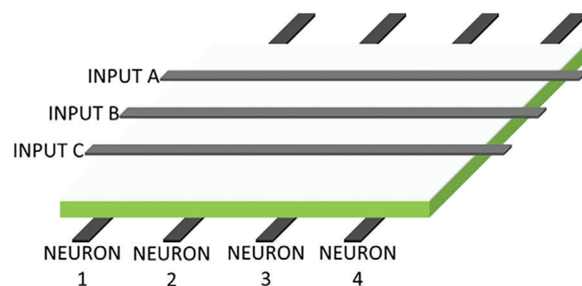

Figure 1. Schematic drawing of the 4 × 3 crossbar sample architecture. From top to bottom: Co electrodes (10 nm thick) corresponding to inputs A,B, and C (grey), AlOx (2 nm thick) tunnel barrier (light grey), Gaq3 molecular thin film (10 nm thick, green), bottom LSMO electrodes (20 nm thick, dark grey), corresponding to neurons 1,2,3 and 4. The devices (i.e., synapses) are the cross-points between the top and the bottom electrodes.

2. Results and Discussion

We fabricated 2 types of crossbar samples, as detailed in the "Methods" section. The first type had 4 bottom LSMO electrodes and 3 top Co electrodes (referred to as 4 × 3 devices). The second type had 3 bottom LSMO electrodes and 1 top Co electrode (referred to as 3 × 1 devices).

Figure 1 shows the basic structure of a 4 × 3 crossbar device. The top Co electrodes and the bottom LSMO ones sandwich the Gaq3 molecular thin film and the AlOx tunnel barrier. Devices (i.e., synapses) correspond to the cross-points between the top and the bottom electrodes.

Figure 2 shows the conductance map of a crossbar device at 76 K; Figure 2a) shows the synapse corresponding to Neuron 2-Input B, in its potentiated state, obtained by the application of +3 V to the bottom LSMO electrode relative to the top Co. In this high conductance state, we could measure a spin valve-like magnetoresistance, that is a conductance that depends on the relative orientation of the magnetizations of the LSMO and the Co electrodes, as shown in Figure 2b). In Figure 2c) we show the same synapse in the depressed state, after the application of −3 V. In this lower conductance state, no spin valve magnetoresistance could be measured (Figure 2d). The presence of the spin valve magnetoresistance in the potentiated state and its absence in the depressed one was consistent with previous experiments on single devices.[19]

To ensure that a crossbar can perform as a whole there are some basic requirements to be met. Among them, there is the ability to address each cross-point separately. This requires the presence of a threshold voltage, which is present in our devices: the resistive state of the devices was not affected by voltages that did not exceed a threshold level, −1 V for depression and +1.75 V potentiation. This is important in order to potentiate or depress each synapse in the crossbar separately because it allows the implementation of the "V/2" scheme (see Methods section). This scheme ensures that only the cross-point of interest experiences a voltage above the threshold, while the remaining ones experience a below-threshold voltage.[20]

Another important aspect is the absence of sneak-paths:[21] the application of a potentiation or depression voltage pulse on the desired cross-point can be hampered by the existence of alternative, high-conductivity current paths. This problem is mitigated

© 2024 The Authors. Advanced Electronic Materials published by Wiley-VCH GmbH

2199160x, 2024, 8, Downloaded from https://onlinelibrary.wiley.com/doi/10.1002/aelm.202300887 by CochraneItalia, Wiley Online Library on [25/11/2024]. See the Terms and Conditions (https://onlinelibrary.wiley.com/terms-and-conditions) on Wiley Online Library for rules of use; OA articles are governed by the applicable Creative Commons License

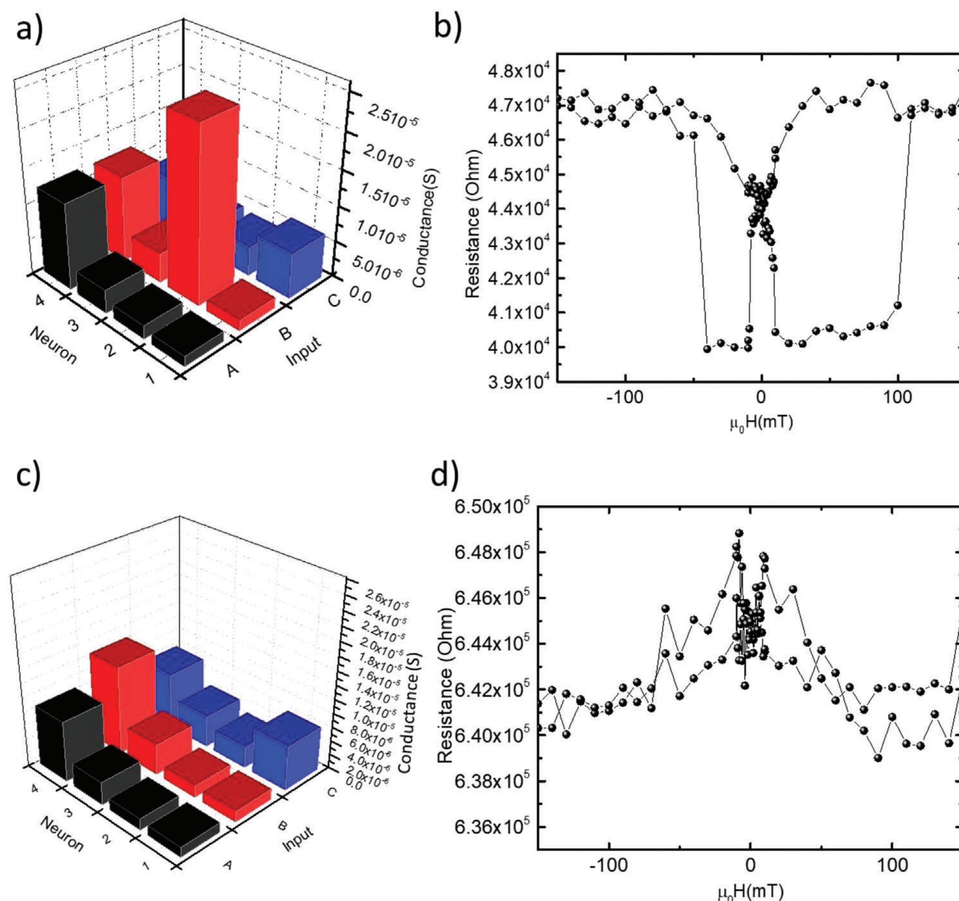

Figure 2. Conductance map of a 4 × 3 crossbar sample, with potentiation and depression of a selected synapse and corresponding magnetoresistance, taken at 76 K by applying 100 mV. a) Potentiation of synapse Neuron2-InputB b) Corresponding magnetoresistance: a spin valve magnetoresistance be detected in the potentiated state c) Depression of the same synapse d) In the depressed the spin valve magnetoresistance disappears.

in our devices by the highly non-linear nature of their current-voltage characteristics (see Figure S1 Supporting Information): if a device is not directly addressed, the use of the "V/2" protocol ensures that the current is very low, effectively switching off all unwanted current paths.

Each synapse of the crossbar shows magnetoresistance in the high conductance state and no magnetoresistance in the low conductance state. (see the "Conductance maps" section of the Supporting Information). In Figure 2 we showed their extremal behavior, that is the magnetoresistance of a synapse in its maximally and its minimally conductive states respectively, with a maximum on/off ratio of $\approx 10^4$ (see the "ON/OFF ratio" section of the Supporting Information). Single devices demonstrated also intermediate states,[15,19,22] which are important for neuromorphic computing, as they allow the tuning of the synaptic weight with a concomitant change in the magnetoresistance.[17] We tested the ability of the synapses to be tuned almost continuously also in the present 4 × 3 crossbar architecture. This behavior has the potential to speed up the learning phase in artificial intelligence applications.[17] The reason for this speed-up is the following. In the depressed, low-conductance state, the magnetoresistance vanishes and the magnetic field does not affect the conductance of the synapse. Instead, when the synapse is potentiated by increasing its conductance, the magnetoresistance is gradually recovered and the conductance can again be affected by the magnetic field. This means that potentiated synapses can be selectively further potentiated by the application of a suitable magnetic field while leaving the depressed synapses unaffected; this mechanism is responsible for the speed-up of the learning phase.

To fully understand the potential of the molecular spintronic devices for neuromorphic computing it is important to study dynamic properties of their response to potentiation and depression pulses. This also sheds light on the similarities and differences of molecular spintronic devices compared to other approaches.

We concentrated on 2 different aspects of the resistive switching dynamics of our molecular spintronic devices, because of their physical and technological relevance. On the one hand, we studied how the conductance responded to pulses of different duration, to understand what the characteristic times of the resistive switching process were. On the other hand, we studied the relaxation of the conductance after a pulse was applied, to understand what happens to the conductive state of our artificial synapses over time.

For the response to pulses of different durations, **Figure 3** shows the incremental change of the conductance of a device at 76 K after the repeated application of 50 identical voltage pulses

© 2024 The Authors. Advanced Electronic Materials published by Wiley-VCH GmbH
2199160x, 2024, 8, Downloaded from https://onlinelibrary.wiley.com/doi/10.1002/aelm.202300887 by CochraneItalia, Wiley Online Library on [25/11/2024]. See the Terms and Conditions (https://onlinelibrary.wiley.com/terms-and-conditions) on Wiley Online Library for rules of use; OA articles are governed by the applicable Creative Commons License

2199160x, 2024, 8, Downloaded from https://onlinelibrary.wiley.com/doi/10.1002/aelm.202300887 by CochraneItalia, Wiley Online Library on [25/11/2024]. See the Terms and Conditions (https://onlinelibrary.wiley.com/terms-and-conditions) on Wiley Online Library for rules of use; OA articles are governed by the applicable Creative Commons License

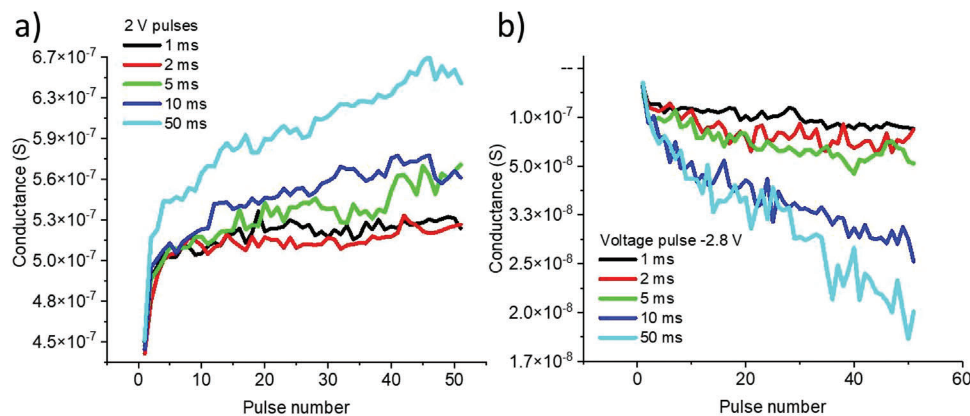

Figure 3. Response of a 4 × 3 sample devices' conductance to repeated identical pulses, taken at 76 K and measured at 100 mV. a) Conductance as a function of pulse number, after the repeated application of identical pulses with a +2 V amplitude and 1, 2, 5, 10, and 50 ms duration b) Conductance as a function of pulse number after repeated, identical −2.8 V pulses, with duration as in a).

of +2 V (Figure 3a)) and −2.8 V (Figure 3b)), with durations of 1, 2, 5, 10, and 50 ms; after each train of pulses the device was reset by the application a sufficiently large voltage of opposite polarity (e.g., −4 V after +2 V pulses and +4 V after −2.8 V pulses) for 1 s. The positive pulses caused synaptic potentiation overall, while negative ones caused depression of the synapse. Longer pulses had a greater effect than shorter ones. The first several pulses lead to the greatest change in conductance, with the subsequent pulses giving smaller and smaller changes, without reaching saturation even after 50 pulses. This slow conductivity dynamics was more pronounced for longer pulses.

The dynamic range of the data reported in Figure 3 is ≈50% for the potentiation pulses and 500% for the depression ones. These values do not correspond to the on/off ratio of the devices, which is much greater; to measure the on/off ratio, we applied voltage pulses that would drive the conductance state to its extremal values with just 1 pulse as in **Figure 4a**), without the possibility to modify the resistive state gradually as in Figure 3. In any case, our dynamic range compares well with the on/off ratio of 50% to 100% of SOT and STT MRAMs for neuromorphic computing.[23]

The logarithmic behavior of the conductance as a function of the number of applied voltage pulses reported in Figure 3 belongs to the non-linear soft-bound (NL-SB) class of non-linear synaptic update rules studied in Brivio et al.[18] There, the NL-SB synapse is shown to give memory storage advantages over linear ones in spiking neural networks (SNNs). In greater detail,

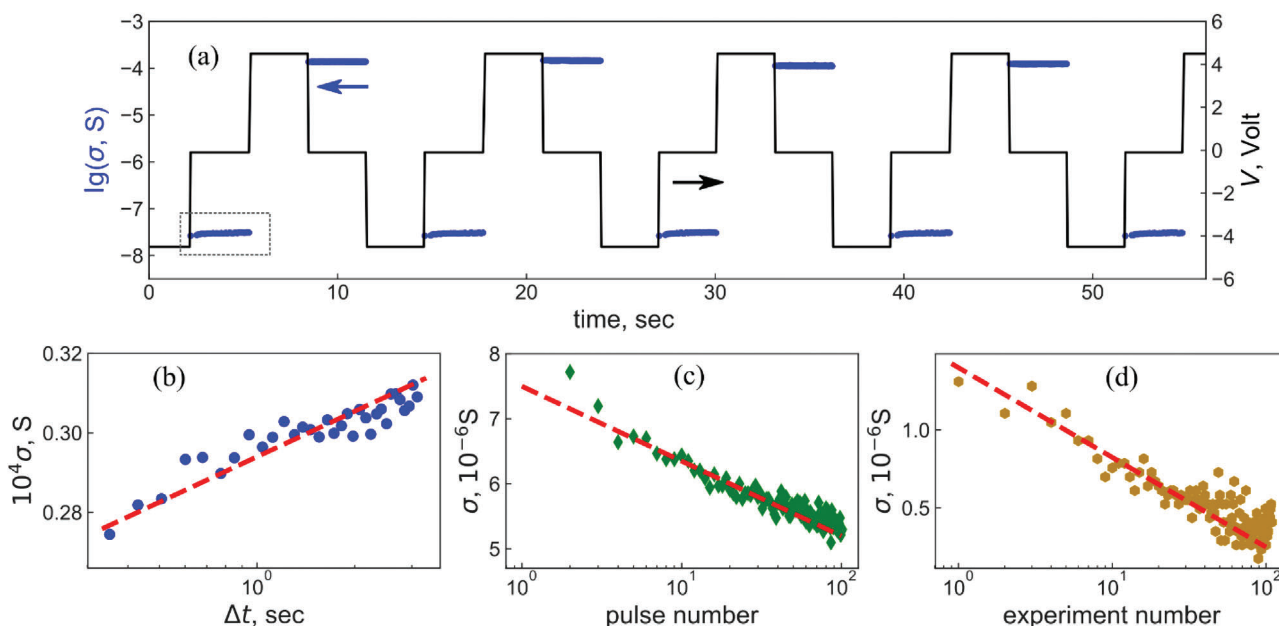

Figure 4. The slow dynamics of conductivity. a) The response of a 3 × 1 sample to a series of +4 V and −4 V pulses taken at 100 K; the duration of the pulses was 3 s, while reading in between lasted for 3 s and was carried out at −100 mV. b) The detailed plot of one such response (dashed rectangle in the panel (a)) compared with the logarithmic increase. c) The conductivity after −3 V, 1 ms duration pulses applied to a device in a 4 × 3 sample. d) The conductivity of a device in a 4 × 3 sample at the beginning of each experiment of the type reported in Figure 3, after a −4 V, 1 s duration reset pulse.

 © 2024 The Authors. Advanced Electronic Materials published by Wiley-VCH GmbH

Brivio et al. show that in general memristive conductance dynamics usually follows a non-linear evolution with a slow approach to the maximum and minimum values,[25,26] as in the devices studied in this article. Such dynamics can be described by a NL-SB model, which is of special importance in the field of computational neuroscience. Fusi and Abbott[27] demonstrated that NL-SB synapses generally give SNNs a larger storage capacity compared to synapses whose weight evolves linearly between 2 limiting values, which are known as linear hard-bound (LHB) synapses. In addition, Gokmen et al.[28] demonstrate that a nonlinear synaptic update rule can be exploited in the so-called "tika-taka" algorithm, achieving a training efficiency comparable to that obtained with linear update rules, on a long-short term memory network, a convolutional neural network, and a fully connected network.

The dependence of the switching behavior on the pulse duration is a universal feature of resistive memories based on widely different technologies.[29,30] It also demonstrates how an electrical field affects ionic transport in valence change memories.[30] Pulses with specific durations and voltages affect maximally the resistive state of the devices.[17] The response to pulses of different lengths is very important for spike time-dependent plasticity, which is based on pulse duration.[14,31]

The pulse generator could not provide pulses shorter than 1 ms, but this is by no means a physical limitation of the devices. In any case, the write time is not the greatest concern for neuromorphic computing, and pulse durations between 0.1 ms and 50 ms are considered acceptable.[20,23,32] Speed is instead crucial in the inference phase, where crossbars have a great advantage as they can perform one-shot vector by matrix multiplication.[20]

To study the slow dynamics of transport properties after the application of potentiation or a depression pulse, we carried out time-resolved measurements of conductivity. For these measurements, in addition to 4 × 3 devices, we also used 3 × 1 devices in order to control for the effects of crosstalk (see the "Quantification of crosstalk" section of the Supporting Information). Figure 4a) shows the response of a device on a 3 × 1 sample at 100 K to a series of alternating positive pulses of +4 V for 3 s and negative pulses of −4 V for 3 s, separated by a 3 s, −100 mV reading voltage phase. The pulses' voltages have a great enough magnitude to set the device in an extremal state (highest possible conductance after +4 V and lower possible conductance after −4 V). While resistive memories in general show considerable cycle-to-cycle variation,[33–35] the conductance reported in Figure 4a) shows remarkable repeatability and stability. The endurance of the devices is demonstrated in Figure S3 (Supporting Information) where, after 5×10^3 set/reset cycles, the on/off ratio shows no sign of degradation, in line with what is reported in the literature.[32]

The small −100 mV reading voltage corresponds to the linear regime, does not affect the resistance state and was thus used to measure the conductivity; during its application, we observed conductivity relaxation over 3 s: when the device is set in the high conductance state, it relaxes to a slightly lower conductance while, on the contrary, when it is set in the low conductance state, it relaxes to a slightly higher conductance level. The blue circles in Figure 4b) show in detail such a relaxation after one depression pulse, while the red dashed line represents a logarithmic increase with time: $\sigma(t) = \sigma_0 + \sigma_1 \log(t)$. Resistive drift after a voltage pulse was observed in several other systems.[36] While it can be detrimental to information storage, it can be useful in learning algorithms that use eligibility traces.[37]

This conductivity relaxation is similar to the slow resistance variations during the series of pulses in Figure 3. Figure 4c), green diamonds, shows the response of a device on a 4 × 3 sample to a series of negative −3 V depression pulses, which can also be described with the logarithmic law $\sigma = \sigma_0 - \sigma_1 \log(N_p)$ where N_p is the pulse number, over a time scale of ≈400 s (red dashed line).

Finally, we also studied the slow time dynamics of the conductance at even larger time scales, as the pulse experiments in Figure 3 were repeated. To do this we plotted the conductance right after the initial reset pulse of several of the experiments reported in Figure 3, as a function of each experiment repetition. Figure 4d) considers the series of potentiation pulse experiments with voltages from +3 V to +4 V and different durations. The experiments were separated by −4 V initial reset pulses. The brown circles in Figure 4d) correspond to conductivity measurements immediately after these initial reset pulses, before the sample was affected by the potentiation voltage pulses. Also, in this case, the dependence on the experiment number can be described as a logarithm $\sigma = \sigma_0 - \sigma_1 \log(N_{exp})$ where N_{exp} is the number of the experiment (red dashed line). With each experiment lasting ≈400 s, the logarithmic dependence in Figure 4d) corresponds to a timescale of 10^5 s.

On the whole, the response on the applied pulses is accompanied by a slow logarithmic relaxation of the conductivity at timescales from 3 to 10^5 s. This dynamic is affected by the electric pulses and is not necessarily present at all the timescales. For example, in the situation shown in Figure 4d) the slow dynamics after the ON pulses were not pronounced in comparison to the dynamics due to erasing pulses (see the "Protocol of the pulse series experiments" section of the Supporting Information for the details).

The logarithmic relaxation of some properties observed in a wide range of time scales is often attributed to the "glassy" dynamics in the material that can be either due to the structural glass[38] or to more exotic spin[39] or Coulomb glasses.[40] A "glassy" physics can be described by a set of energy barriers with a flat distribution function that a particle (electron or atom) should overcome either by tunneling or thermal activation.[41]

To understand the specifics of the glassy behavior in our devices we consider the model from Riminucci et al.[19] The conductivity at low voltage is provided by oxygen impurities in Gaq3. However, the sample resistance is controlled by Schottky barriers (space-charge regions) where the energy level of the impurities is far from the Fermi level. These regions form the tunneling barriers for the electrons (see **Figure 5a**). The transport occurs mostly in thin filaments with increased concentrations of oxygen and probably the weak points in the barriers. The voltage pulses affect the conductivity due to the electromigration of impurities that lead to the modification of oxygen concentration and their re-arrangement.

The atomic electromigration is well-studied in crystalline solids where it is usually related to the overcoming of the barriers ≈1 eV with thermal activation.[42] There are indications that in organics some barriers can be much smaller, e.g. ≈0.2 eV.[43]

© 2024 The Authors. Advanced Electronic Materials published by Wiley-VCH GmbH

2199160x, 2024, 8, Downloaded from https://onlinelibrary.wiley.com/doi/10.1002/aelm.202300887 by CochraneItalia, Wiley Online Library on [25/11/2024]. See the Terms and Conditions (https://onlinelibrary.wiley.com/terms-and-conditions) on Wiley Online Library for rules of use; OA articles are governed by the applicable Creative Commons License

2199160x, 2024, 8, Downloaded from https://onlinelibrary.wiley.com/doi/10.1002/aelm.202300887 by Cochraneltalia, Wiley Online Library on [25/11/2024]. See the Terms and Conditions (https://onlinelibrary.wiley.com/terms-and-conditions) on Wiley Online Library for rules of use; OA articles are governed by the applicable Creative Commons License

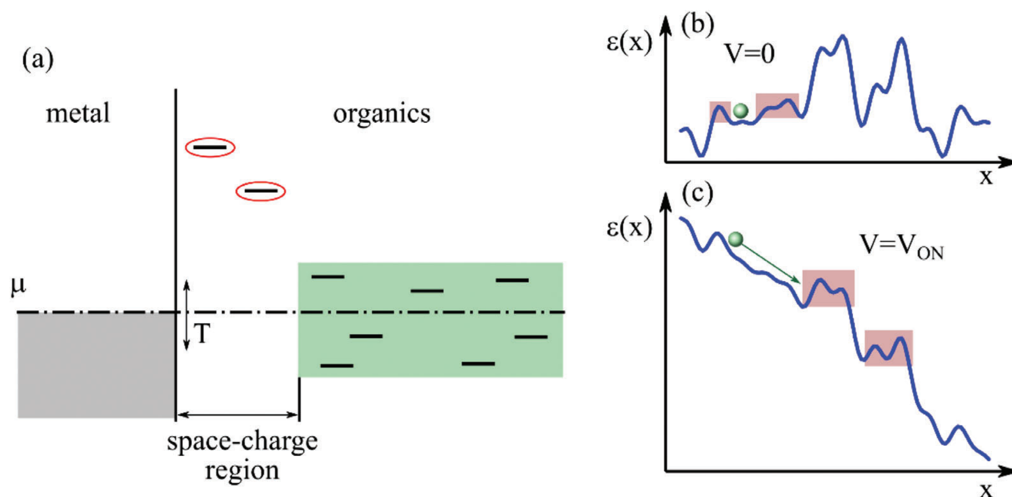

Figure 5. The glassy dynamics of oxygen impurities and its effect on the device conductivity. a) Electron states at the metal-organic interface. b) The impurity energy landscape as a function of generalized coordinate x between pulses. c) The energy landscape during the pulse.

However, 0.2 eV barriers require an finite applied voltage to be overcome, even above room temperature. We assume that due to the amorphous nature of molecular semiconductors the actual energy barriers have a flat distribution with finite density at zero energy.

The energy landscape for an oxygen impurity can be described by a set of such barriers with heights from 0 to ≈1 eV. We show the cartoon for such a landscape in Figure 5b) where x is a generalized coordinate. Even without an applied voltage, some barriers can be penetrated due to a finite temperature leading to limited oxygen mobility and slow relaxations after the electric pulses (as shown by the rectangles in Figure 5b). During the pulses, a constant slope is added to the landscape (Figure 5c). Some barriers can be smeared leading to impurity transport without activation (green arrow in Figure 5c). However, there could still be some barriers that oxygen cannot overcome with an electric field alone. They require the combined effect of pulses and activation. Such barriers lead to logarithmic relaxation after a series of potentiating or depressing pulses (Figure 3a,b).

3. Conclusion

We have shown that the conductance of LSMO/Gaq3/AlOx/Co molecular spin valves can be modulated gradually by the repeated application of identical voltage pulses. Following prior literature,[19,44] we attribute this behavior to the migration of oxygen species within the Gaq3/AlOx bilayer that creates impurity conduction levels in the Gaq3 film. Such impurities can migrate from the AlOx to the Gaq3 film and back upon the application of a suitable voltage.

The conductance can be gradually increased by the application of positive pulses and gradually decreased by the application of negative ones. This behavior mimics respectively the potentiation and depression processes of a neuron's synapse. In a sample containing 4 × 3 devices arranged in a crossbar configuration, we could address each device separately, with an average crosstalk of 8%. When in the high conductance state, the devices showed magnetoresistance, while in the lower conductance one, the magnetoresistance was not observed; this can lead to accelerated learning.

The change in conductance followed a logarithmic law as a function of time and as a function of the number of applied pulses. We attribute this behavior to a flat distribution of energy barriers to the migration of the oxygen species with the molecular semiconductor film and provide a physical model for it. This logarithmic behavior, known as NL-SB in neuromorphic computing, is known to be advantageous over simpler but less realistic laws, such as LHB.

On the whole, we expect our findings to usher molecular spintronics in the quest for new materials for energy-efficient artificial solid-state synapses.

4. Experimental Section

We fabricated 2 types of crossbar samples. The first type was grown on 10 × 10 × 0.5 mm^3 1 side polished $SrTiO_3$ (100) substrates procured from Crystal GmbH, and had 4 bottom LSMO electrodes and 3 top Co electrodes (referred to as 4 × 3 devices). The second type was grown on 10 × 5 × 0.5 mm^3 1 side polished $SrTiO_3$ (100) substrates, and had 3 bottom LSMO electrodes and 1 top Co electrode (referred to as 3 × 1 devices). As a cleaning procedure, they were sonicated for 10′ in spectroscopic grade acetone, then for 10′ in spectroscopic grade isopropanol. The cleaned substrates were placed in a channel spark ablation chamber, covered with a Pt shadow mask, and heated to a temperature of 865 °C. We then grew the 20 nm thick LSMO stripes, 10 mm long and 1 mm wide, by channel spark ablation in a 2.42×10^{-2} mbar pure O_2 atmosphere.[45,46] The sample was placed in an ultra-high vacuum (UHV) physical vapor deposition system and annealed for 30′ at 250 °C at a 10^{-9} mbar base pressure to recover the LSMO surface properties after exposition to the atmosphere. Without breaking the vacuum we evaporated 10 nm of Gaq3 at a base pressure of 10^{-9} mbar, followed by 2 nm of Al. The Al was oxidized by exposing the sample to a 100 mbar pure oxygen atmosphere for 30′ at room temperature to obtain an AlOx tunnel barrier.[47] Finally, we deposited the 10 nm thick Co electrodes by e-beam evaporation at a base pressure of 10^{-10} mbar. The patterning of the Gaq3, Al, and Co films was performed with an in-situ shadow masking system. The morphology of the LSMO and of the quinoline/AlOx film grown on top of it are reported in Figures S8 and S9 (Supporting Information). Together with the

 © 2024 The Authors. Advanced Electronic Materials published by Wiley-VCH GmbH

cross-sectional study reported by Bergenti et al.[44] these data demonstrate the high quality of the devices.

The finished samples were placed in an Oxford Instruments continuous flow cryostat that was placed between the poles of an electromagnet. To carry out the magnetotransport measurements we used 2 different contacting methods for the programming and for the reading steps, respectively. The programming voltages were applied following the V/2 protocol. This reduces crosstalk between the electrodes of the active and the other ones. Accordingly, in order to have a voltage V applied to a cross-point device, we applied V/2 to the respective neuron electrode and −V/2 to the respective input. The remaining electrodes were kept to ground so that none of the remaining devices felt the full V voltage but only ±V/2. For the reading step, used to determine the conductance of the devices, we applied 0.1 V to the corresponding input and read the current on the corresponding neuron via a virtual ground with a Keithley 2450 source measure unit; the remaining electrodes were put to the ground.[20]

Supporting Information

Supporting Information is available from the Wiley Online Library or from the author.

Acknowledgements

The authors would like to thank Federico Bona for his invaluable technical contribution. AS, AR, IB, MS, RR, LG, MB, and AD acknowledge funding from EU FET Open projects SINFONIA (G.A. 964396) and INTERFAST (G.A. 965046). AR, IB, and RC also acknowledge funding from PRIN PNRR 2022 project CAMOUFLAGE (C.U.P. P2022AXCXZ).

Conflict of Interest

The authors declare no conflict of interest.

Data Availability Statement

The data that support the findings of this study are available from the corresponding author upon reasonable request.

Keywords

glassy dynamics, molecular spintronics, neuromorphic computing

Received: December 19, 2023
Revised: February 15, 2024
Published online: April 1, 2024

[1] M. Flasiński, in *Introduction to Artificial Intelligence.*, (Ed: M. Flasiński), Springer International Publishing, Cham, **2016**, 15.
[2] J. A. Hertz, *Introduction To The Theory Of Neural Computation*, CRC Press, Boca Raton, **2019**.
[3] "Neuromorphic computing," https://www.nature.com/collections/cdadajcjjc, **2020**.
[4] G. M. Shepherd, G. M. Shepherd, Eds., *The Synaptic Organization of the Brain*, Oxford University Press, Oxford, New York, **2004**.
[5] Y. LeCun, B. Boser, J. S. Denker, D. Henderson, R. E. Howard, W. Hubbard, L. D. Jackel, *Neural Comput* **1989**, *1*, 541.
[6] P. Mannocci, M. Farronato, N. Lepri, L. Cattaneo, A. Glukhov, Z. Sun, D. Ielmini, *APL Mach. Learn.* **2023**, *1*, 010902.
[7] D. Ielmini, S. Ambrogio, *Nanotechnology* **2019**, *31*, 092001.
[8] D. Ielmini, *Microelectron. Eng.* **2018**, *190*, 44.
[9] D. V. Christensen, R. Dittmann, B. Linares-Barranco, A. Sebastian, M. L. Gallo, A. Redaelli, S. Slesazeck, T. Mikolajick, S. Spiga, S. Menzel, I. Valov, G. Milano, C. Ricciardi, S.-J. Liang, F. Miao, M. Lanza, T. J. Quill, S. T. Keene, A. Salleo, J. Grollier, D. Marković, A. Mizrahi, P. Yao, J. J. Yang, G. Indiveri, J. P. Strachan, S. Datta, E. Vianello, A. Valentian, J. Feldmann, et al., *Neuromorphic Comput. Eng.* **2022**, *2*, 022501.
[10] M. L. Gallo, A. Sebastian, *J. Phys. Appl. Phys.* **2020**, *53*, 213002.
[11] A. Gruverman, B. J. Rodriguez, C. Dehoff, J. D. Waldrep, A. I. Kingon, R. J. Nemanich, J. S. Cross, *Appl. Phys. Lett.* **2005**, *87*, 082902.
[12] R. Waser, R. Dittmann, G. Staikov, K. Szot, *Adv. Mater.* **2009**, *21*, 2632.
[13] S. Brivio, S. Spiga, D. Ielmini, *Neuromorphic Comput. Eng.* **2022**, *2*, 042001.
[14] Y. van de Burgt, E. Lubberman, E. J. Fuller, S. T. Keene, G. C. Faria, S. Agarwal, M. J. Marinella, A. Alec Talin, A. Salleo, *Nat. Mater.* **2017**, *16*, 414.
[15] M. Prezioso, A. Riminucci, I. Bergenti, P. Graziosi, D. Brunel, V. A. Dediu, *Adv. Mater.* **2011**, *23*, 1371.
[16] M. Prezioso, A. Riminucci, P. Graziosi, I. Bergenti, R. Rakshit, R. Cecchini, A. Vianelli, F. Borgatti, N. Haag, M. Willis, A. J. Drew, W. P. Gillin, V. A. Dediu, *Adv. Mater.* **2013**, *25*, 534.
[17] A. Riminucci, R. Legenstein, *arXiv* **2019**, *1903*, 08624.
[18] S. Brivio, D. R. B. Ly, E. Vianello, S. Spiga, *Front. Neurosci.* **2021**, *15*.
[19] A. Riminucci, Z.-G. Yu, M. Prezioso, R. Cecchini, I. Bergenti, P. Graziosi, V. A. Dediu, *ACS Appl. Mater. Interfaces* **2019**, *11*, 8319.
[20] M. Prezioso, F. Merrikh-Bayat, B. D. Hoskins, G. C. Adam, K. K. Likharev, D. B. Strukov, *Nature* **2015**, *521*, 61.
[21] L. Shi, G. Zheng, B. Tian, B. Dkhil, C. Duan, *Nanoscale Adv* **2020**, *2*, 1811.
[22] M. Prezioso, A. Riminucci, P. Graziosi, I. Bergenti, R. Rakshit, R. Cecchini, A. Vianelli, F. Borgatti, N. Haag, M. Willis, A. J. Drew, W. P. Gillin, V. A. Dediu, *Adv. Mater.* **2013**, *25*, 534.
[23] V. Milo, G. Malavena, C. Monzio Compagnoni, D. Ielmini, *Materials* **2020**, *13*, 166.
[24] M. L. Perrin, E. Burzurí, H. S. J. van der Zant, *Chem. Soc. Rev.* **2015**, *44*, 902.
[25] A. Fumarola, S. Sidler, K. Moon, J. Jang, R. M. Shelby, P. Narayanan, Y. Leblebici, H. Hwang, G. W. Burr, *IEEE J. Electron Devices Soc.* **2018**, *6*, 169.
[26] J. Frascaroli, S. Brivio, E. Covi, S. Spiga, *Sci. Rep.* **2018**, *8*, 7178.
[27] S. Fusi, L. F. Abbott, *Nat. Neurosci.* **2007**, *10*, 485.
[28] T. Gokmen, W. Haensch, *Front. Neurosci.* **2020**, *14*.
[29] N. Lyapunov, X. D. Zheng, K. Yang, H. M. Liu, K. Zhou, S. H. Cai, T. L. Ho, C. H. Suen, M. Yang, J. Zhao, X. Zhou, J.-Y. Dai, *Adv. Electron. Mater.* **2022**, *8*, 2101235.
[30] F. Cüppers, S. Menzel, C. Bengel, A. Hardtdegen, M. von Witzleben, U. Böttger, R. Waser, S. Hoffmann-Eifert, *APL Mater.* **2019**, *7*, 091105.
[31] M. Prezioso, F. Merrikh Bayat, B. Hoskins, K. Likharev, D. Strukov, *Sci. Rep.* **2016**, *6*, 21331.
[32] S. G. Kim, J. S. Han, H. Kim, S. Y. Kim, H. W. Jang, *Adv. Mater. Technol.* **2018**, *3*, 1800457.
[33] G. Piccolboni, G. Molas, D. Garbin, E. Vianello, O. Cueto, C. Cagli, B. Traore, B. De Salvo, G. Ghibaudo, L. Perniola, *IEEE Electron Device Lett.* **2016**, *37*, 721.
[34] M. Rizzi, N. Ciocchini, A. Montefiori, M. Ferro, P. Fantini, A. L. Lacaita, D. Ielmini, *IEEE Trans. Electron Devices* **2015**, *62*, 2205.
[35] J. B. Roldán, E. Miranda, D. Maldonado, A. N. Mikhaylov, N. V. Agudov, A. A. Dubkov, M. N. Koryazhkina, M. B. González, M. A. Villena, S. Poblador, M. Saludes-Tapia, R. Picos, F. Jiménez-Molinos, S. G. Stavrinides, E. Salvador, F. J. Alonso, F. Campabadal, B. Spagnolo, M. Lanza, L. O. Chua, *Adv. Intell. Syst.* **2023**, *5*, 2200338.

© 2024 The Authors. Advanced Electronic Materials published by Wiley-VCH GmbH

2199160x, 2024, 8, Downloaded from https://onlinelibrary.wiley.com/doi/10.1002/aelm.202300887 by CochraneItalia, Wiley Online Library on [25/11/2024]. See the Terms and Conditions (https://onlinelibrary.wiley.com/terms-and-conditions) on Wiley Online Library for rules of use; OA articles are governed by the applicable Creative Commons License

[36] S. R. Nandakumar, M. L. Gallo, I. Boybat, B. Rajendran, A. Sebastian, E. Eleftheriou, *J. Appl. Phys.* **2018**, *124*, 152135.
[37] Y. Demirağ, F. Moro, T. Dalgaty, G. Navarro, C. Frenkel, G. Indiveri, E. Vianello, M. Payvand, in *2021 IEEE Int. Symp. Circuits Syst. (ISCAS)* May **2021**, 1.
[38] J. M. Hutchinson, *Prog. Polym. Sci.* **1995**, *20*, 703.
[39] K. Binder, A. P. Young, *Phys. Rev. B* **1984**, *29*, 2864.
[40] J. Bergli, Y. M. Galperin, *Phys. Rev. B* **2012**, *85*, 214202.
[41] A. Amir, Y. Oreg, Y. Imry, *Proc. Natl. Acad. Sci* **2012**, *109*, 1850.
[42] D. G. Pierce, P. G. Brusius, *Microelectron. Reliab.* **1997**, *37*, 1053.
[43] Y. Tomita, T. Nakayama, *Org. Electron.* **2012**, *13*, 1487.
[44] I. Bergenti, F. Borgatti, M. Calbucci, A. Riminucci, R. Cecchini, P. Graziosi, D. A. MacLaren, A. Giglia, J. P. Rueff, D. Céolin, L. Pasquali, V. Dediu, *ACS Appl. Mater. Interfaces* **2018**, *10*, 8132.
[45] P. Graziosi, M. Prezioso, A. Gambardella, C. Kitts, R. K. Rakshit, A. Riminucci, I. Bergenti, F. Borgatti, C. Pernechele, M. Solzi, D. Pullini, D. Busquets-Mataix, V. A. Dediu, *Thin Solid Films* **2013**, *534*, 83.
[46] V. A. Dediu, J. López, F. C. Matacotta, P. Nozar, G. Ruani, R. Zamboni, C. Taliani, *Phys. Status Solidi B* **1999**, *215*, 625.
[47] F. Borgatti, I. Bergenti, F. Bona, V. Dediu, A. Fondacaro, S. Huotari, G. Monaco, D. A. MacLaren, J. N. Chapman, G. Panaccione, *Appl. Phys. Lett.* **2010**, *96*, 043306.

© 2024 The Authors. Advanced Electronic Materials published by Wiley-VCH GmbH

2199160x, 2024, 8, Downloaded from https://onlinelibrary.wiley.com/doi/10.1002/aelm.202300887 by CochraneItalia, Wiley Online Library on [25/11/2024]. See the Terms and Conditions (https://onlinelibrary.wiley.com/terms-and-conditions) on Wiley Online Library for rules of use; OA articles are governed by the applicable Creative Commons License